ADVANCED FUNCTIONAL MATERIALS
www.afm-journal.de

Tumor Microenvironment-Activatable Nanoenzymes for Mechanical Remodeling of Extracellular Matrix and Enhanced Tumor Chemotherapy

Yinan Zhong, Jianguang Zhang, Junmei Zhang, Yong Hou, Enping Chen, Dechun Huang, Wei Chen,* and Rainer Haag**

Increased tissue stiffness is a hallmark of cancer and promotes tumor progression. It is hypothesized that decreased tumorous stress may aid or sensitize chemotherapies. To overcome extracellular matrix (ECM) stiffening and fulfill sensitized chemotherapy in one nanosystem, a reactive oxygen species-activatable nanoenzyme (SP-NE) based on a dendritic polyglycerol scaffold, integrating collagenase and paclitaxel (PTX) prodrug, is constructed. The dense and tough ECM is highly remitted by SP-NE in the tumor microenvironment (TME) mimicking gelatin hydrogel models, which causes cell shrinkage, disorders cytoskeletal constructions, and subsequently enhances chemotherapeutic efficacy. ECM softening via SP-NE downregulates mechanotransduction signaling pathways of integrin-focal adhesion kinase (FAK)-Ras homolog family member A (RhoA) implicated in cytoskeletal assembly, and integrin-FAK-phosphorylated extracellular signal regulated kinase (pERK 1/2) mediating mitosis. Notably, this programmed nanosystem in human breast MCF-7 tumor-bearing mice models displays a significant relief of ECM stress from 4300 to 1200 Pa and results in 87.1% suppression of tumor growth at a low PTX dosage of 3 mg kg^{-1}. The attenuated expression of the key players RhoA and pERK 1/2 involved in cellular mechanosensing is further verified in vivo. This study thus provides a new and potential nanoplatform to selectively decrease TME stiffness for enhanced chemotherapy.

1. Introduction

Nanomedicines for anti-cancer applications have been perplexed by compromised therapeutic benefits in clinic for a long time.[1–4] It is increasingly recognized that one of the major causes for the failure of nanomedicines in clinic is the complicated and unique biology of tumor microenvironment (TME),[5,6] which consists of tumorous extracellular matrix (ECM), tumor associated fibroblasts, growth factors, vasculature, as well as immune cells.[7–9]

As one of the pivotal features of tumor micromilieu, the mechanical stiffness in tumor contexts is typically higher than that in healthy tissues,[10,11] which is utilized as the basis for manual palpation and mammographic density screening in clinical diagnosis of breast cancer.[12] The increased breast tissue rigidity is always linked with an elevated risk of high malignancy, as well as poor prognosis in cancer patients.[13,14] On a cellular level, matrix stiffness as an external input, regulates integrin clustering, focal adhesion formation, cytoskeletal meshwork and the morphogenesis via activating a cascade of mechanical feedback loops, guiding cell behavior and even determining cell fate.[15,16] The signaling cascade includes Ras homolog (Rho) family guanosine triphosphatases such as RhoA, which modulates actin assembly and induces cell survival. Additionally, mitogen-activated protein kinase-extracellular signal-regulated kinase (MAPK-ERK) pathway, which is involved in mitosis and cell proliferation, is also initiated when receiving extrinsic mechanical cues.[17] Of late, both of RhoA and ERK have been reported to play a role in sensitizing cancer cells to chemotherapy.[18,19] Therefore, it is speculated that decreasing the solid stress in TME may favor or sensitize chemotherapy via altering the cellular priming state.

Recently, a multitude of efforts have been devoted to normalization or modulation of TME for enhanced tumor penetration,[20–22] promoted nanoparticle accessibility to cancer cells,[23] improved drug delivery within tumors,[24] as well as relief of tumor hypoxic and immunosuppressive conditions.[25–27]

Dr. Y. Zhong, J. Zhang, E. Chen, Prof. D. Huang, Prof. W. Chen
Department of Pharmaceutical Engineering
China Pharmaceutical University
Nanjing 211198, China
E-mail: ynzhong@cpu.edu.cn, zhongyinan@126.com; w.chen@cpu.edu.cn
Dr. Y. Zhong, Dr. J. Zhang, Dr. Y. Hou, Prof. R. Haag
Institut für Chemie und Biochemie
Freie Universität Berlin
Takustr. 3, Berlin 14195, Germany
E-mail: haag@chemie.fu-berlin.de
The ORCID identification number(s) for the author(s) of this article can be found under https://doi.org/10.1002/adfm.202007544.

DOI: 10.1002/adfm.202007544

However, mechanical remodeling of tumorous ECM for enhanced cancer chemotherapeutic response in one nanosystem and the potential underlying mechanism remains elusive. The tumorous ECM stiffening is attributed to several factors including overproduction of ECM components (collagens, fibronectins, proteoglycans), and elevated expression of lysyl oxidase, which mediates covalently intra- and intermolecular crosslinking of collagens.[28,29] The protease enzyme collagenase, which can effectively digest collagen, was reported to efficiently modify the dense and tough structure of ECM for promoted tumor penetration of nanoparticles or antibodies, resulting in enhanced chemo-, photodynamic, and antibody therapies.[30–32] Different from the above, in our mechanical remodeling of TME to sensitize chemotherapeutics strategy, the aim of collagenase digestion of ECM is to research the effect of different quantified tumor mechanical modulus on mechanical sensing, cellular response as well as chemotherapy, which is a very new and significant research on dynamic mechano-biology in tumor therapy.

Hence, we construct a TME-responsive nanoenzyme (termed as SP-NE) based on reactive oxygen species (ROS)-responsive dialkynyl-terminated oxalate crosslinked dendritic polyglycerol architectures chaperoning both of collagenase and a pH-sensitive paclitaxel (PTX) prodrug (**Figure 1**a). In the presence of ROS in TME, the nanoenzymes are disassociated owing to the cleavage of dialkynyl-terminated oxalate crosslinker, causing collagenase release in TME for tumor specific relief of the ECM stress and generating PTX prodrug for chemotherapy of mechanical stimulated cancer cells. For nanostructured drug delivery systems, it is for the first time to combine the functions of mechanical remodeling of TME and chemotherapeutics in one single and robust system for enhanced anti-tumor efficacy, subtly realizing programmed mechanical input in TME, cellular mechano-sensing and the consequently enhanced chemotherapy. The effect of nanoenzyme-mediated mechanical alteration on cellular behaviors is investigated using human breast cancer MCF-7 cells seeded on methacrylated gelatin gels. Remarkably, the enhancement of chemotherapeutic efficacy via nanoenzyme-mediated TME softening and the corresponding sensitization of cancer cells are highlighted. To further support our proof of concept, we explore the underlying mechanism and find that nanoenzyme-modified TME interferes the mechanical signaling transduction of integrin-focal adhesion kinase (FAK)-Ras homolog family member A (RhoA) in enhancing actin cytoskeleton dynamics and integrin-FAK-phosphorylated extracellular signal regulated kinase (pERK 1/2) in promoting mitosis, resulting in improved chemosensitivity and treatment outcomes (Figure 1b).

2. Results and Discussions

2.1. Design and Characterization of TME-Activatable Nanoenzymes

Three main components were prepared to fabricate TME-activatable nanogels (SP-NG), containing i) dendritic azido polyglycerol sulfate (dPGS-N_3) with a negative charge for enzyme packaging via electrostatic interaction, ii) pH-sensitive acetal-linked paclitaxel-dendritic azido polyglycerol macromolecular prodrug (dPG(N_3)-ace-PTX) which can release PTX in its pristine nature under endo/lysosomal pH within tumor cells,[33] and iii) the ROS-labile crosslinker dialkynyl-terminated oxalate due to the abundant ROS content in TME.[34] dPGS-N_3 (10 kDa, 82% sulfation, 10% azidation) was synthesized according to a previous work of our group.[35] pH-sensitive vinyl ether acrylate-PTX (VEA-PTX) was obtained via a "click" type coupling between hydroxyl groups of PTX and vinyl ether of VEA, the resultant VEA-PTX was subsequently grafted to the dPG(N_3)-SH backbone (10 kDa, 8% azidation, 1% sulfhydrylation), yielding dPG(N_3)-ace-PTX (Figure S1a, Supporting Information). High-performance liquid chromatography (HPLC) assays revealed a PTX content of about 8.8 wt%. ROS-activatable oxalyl dialkynyl crosslinker was obtained via the reaction between oxalyl chloride and propargyl alcohol (Figure S1b, Supporting Information). The terminal alkynyl groups on both ends of the crosslinkers were readily linked with azide groups of both dPGS-N_3 and dPG(N_3)-ace-PTX, forming a nanoscale polymer network. While the oxalyl ester linker is ROS sensitive and can be cleaved at H_2O_2 concentration of 50 μM.[36,37]

PTX-incorporated nanoenzyme (SP-NE) was generated via nanoprecipitation and in situ incorporation of collagenase by adding the three components in DMSO into an aqueous enzyme solution in phosphate buffer (PB) dropwise. As shown in **Figure 2**a, the size of the nanoarchitectures without enzyme (SP-NG) was about 54 nm determined by dynamic light scattering (DLS); the morphology of SP-NG was a spherical shape with a diameter of about 50 nm visualized under transmission electron microscopy (TEM). The colloidal stability of SP-NG performed well with little size change against 100-fold dilution, as well as in PB containing 10% fetal bovine serum (FBS) or whole blood serum for 12 h incubation (Figure S6, Supporting Information). The tailorable property of the nanocarrier (SP-NG) was tested upon exposure to 50 μM H_2O_2, which mimics ROS-abundant condition in TME. DLS results revealed a remarkable size decrease from 54 to ≈21 nm at 0.5 h (Figure 2b). From TEM graphs, the intact spherical shapes were partially dissociated, accompanying with some newly appeared small-sized dots at 0.5 h incubation upon H_2O_2 (Figure 2b). After another 22 h incubation, considerable small dots with size around several nanometers were observed (Figure 2c). In contrast, the size of SP-NG without H_2O_2 incubation maintained almost the same (Figure 2d). The release kinetics of both FITC-collagenase and paclitaxel from SP-NE were quantified via fluorescence spectrophotometry and HPLC, respectively. SP-NE was subjected to PB at pH 7.4 containing 50 μM H_2O_2 at 37 °C; the release of FITC-collagenase was rapid with enzyme cumulative release of 69% within 24 h incubation, while less than 20% FITC-collagenase leakage was observed under a physiological condition without H_2O_2 (Figure 2e), indicating ROS-responsive cleavage of the crosslinkers and the subsequent efficient enzyme release. In the following, the SP-NE in a H_2O_2-containing media was transferred to acetate buffer with endosomal pH (pH 5.0). A considerably enhanced PTX release of 65% at 48 h was examined, whereas SP-NE displayed a much slower PTX release profile (PTX cumulative release of 18% at

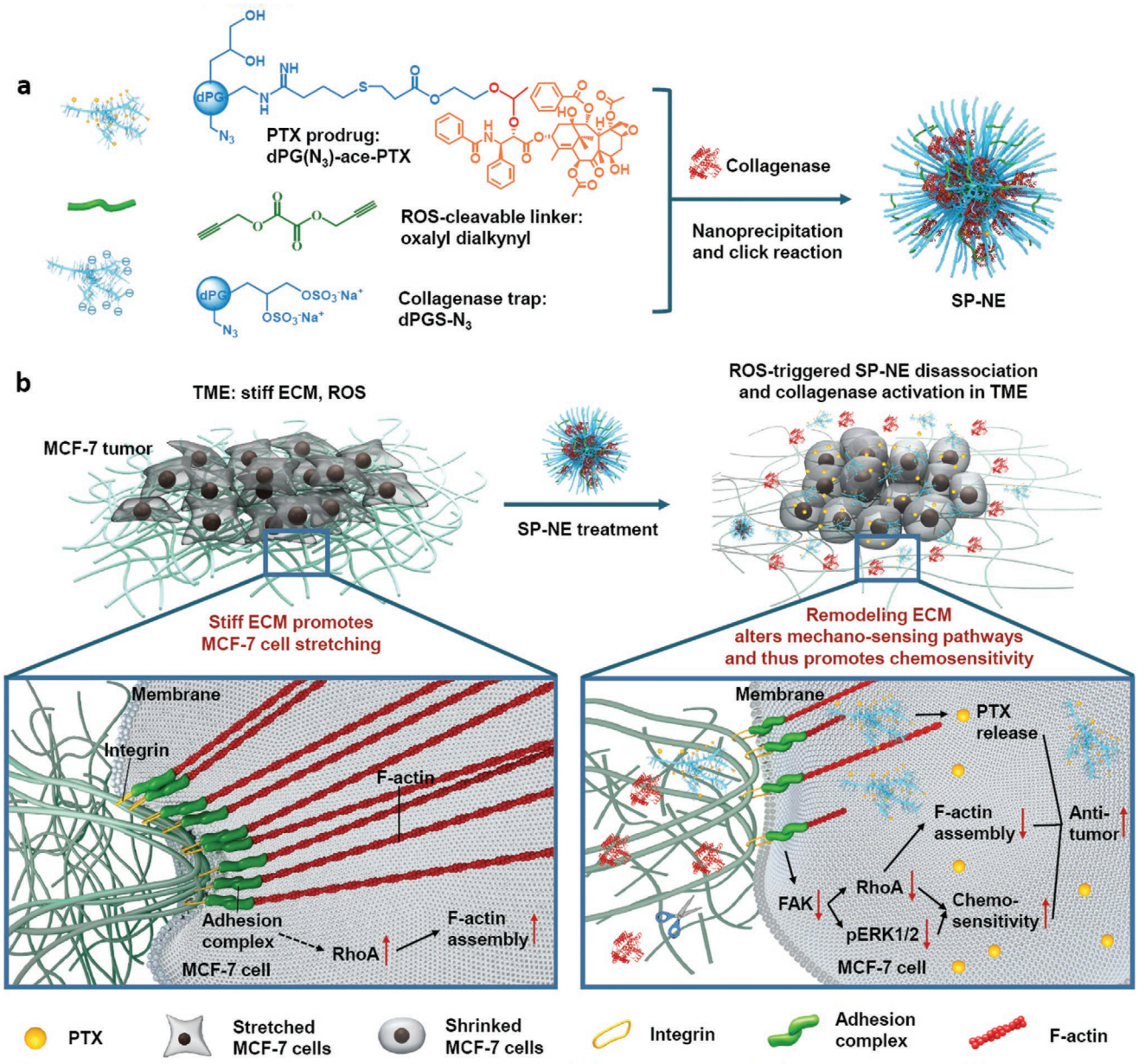

Figure 1. Schematic illustration about a) components and formation of SP-NE, and b) a proposed mechanism of SP-NE-modulated mechanical remodeling of ECM to enhance MCF-7 cells' susceptibility toward chemotherapy: In the presence of ROS in TME, SP-NE is disassociated, resulting in release of collagenase for ECM softening and PTX prodrug for chemotherapy within cells; the dramatically relieved ECM stiffness compromises the mechanical signaling events of integrin-FAK-RhoA involved in enhancing F-actin assembly dynamics and integrin-FAK-pERK 1/2 mediating mitosis, leading to an unfavorable state of cells with shrinked morphologies and dampened cytoskeleton, and improved chemosensitivity.

48 h) at pH 7.4 (Figure 2e). The programmed disassociation of the nanoarchitectures as well as the consequent payload release facilitated enzymatic activities in TME and antitumor activities in tumor cells.

2.2. SP-NE for ECM Mechanical Remodeling and Sensitization in Killing Cells

To investigate the enzymatic activities of dPGS-based nanoenzyme without PTX prodrug (termed as S-NE) and SP-NE on ECM mechanics, a hydrogel based on methacrylated gelatin was adopted as a matrix model for tumor cell culture.[12] The hydrogels with different stiffness were formed by dissolving methacrylated gelatin at different concentrations ranging from 5% to 15% and crosslinking upon UV exposure (365 nm, 10 min) in the presence of catalytic lithium phenyl-2,4,6-trimethyl-benzoyl-phosphinate. The stiffness of 15% hydrogels was determined by rheology with elastic modulus (G') of 5.6 kPa (Figure S9, Supporting Information), which is similar to the stiffness in mammary tumor tissues. In the following in vitro studies, human breast tumor MCF-7 cells were

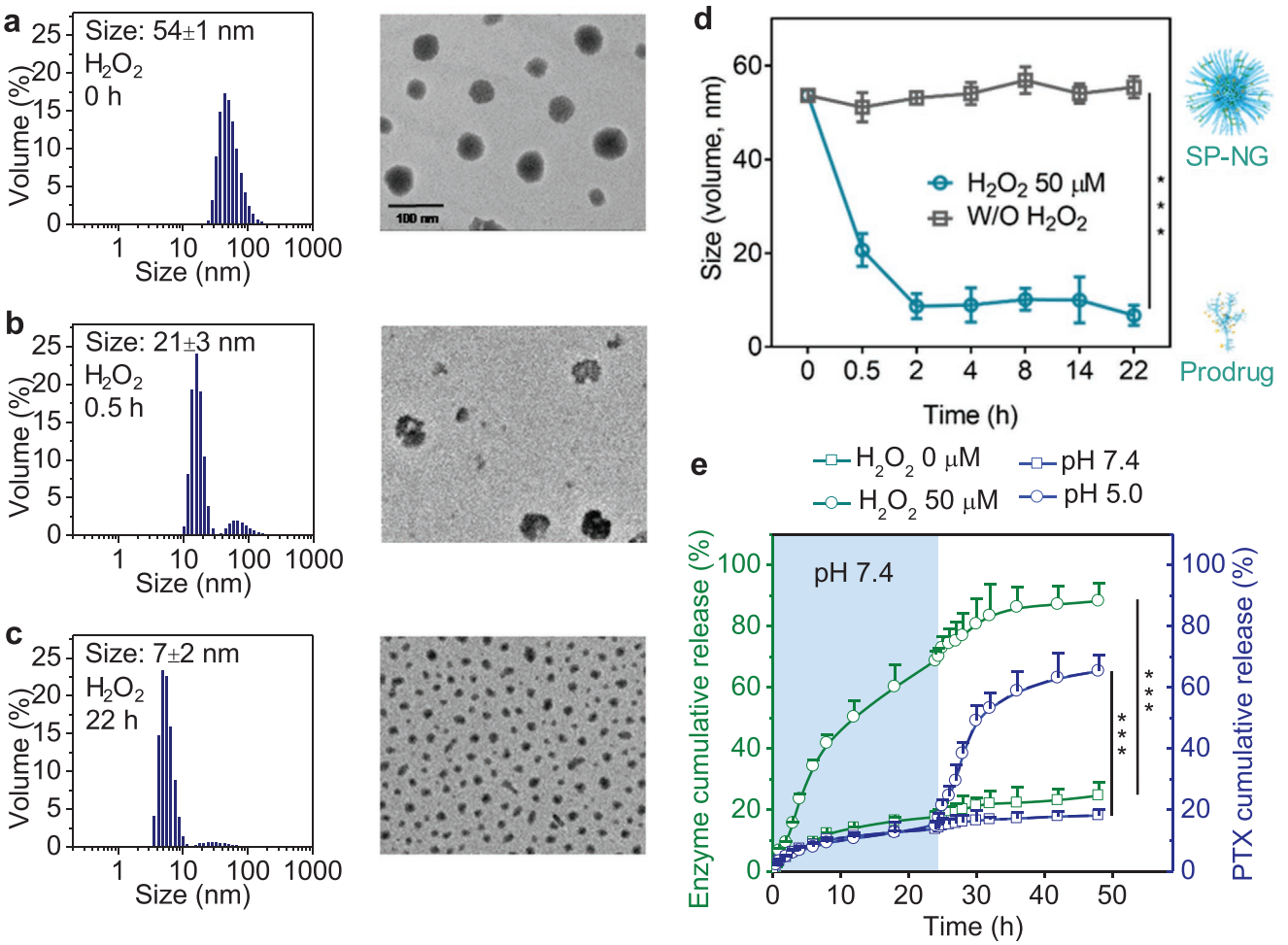

Figure 2. Characterization of SP-NG and SP-NE. a–c) Size change of SP-NG in the media containing 50 μM H_2O_2 at 0 (a), 0.5 (b), and 22 (c) h determined by DLS and TEM. d) Size change of SP-NG in PB without H_2O_2 and PB containing 50 μM H_2O_2 at different time points measured by DLS ($n = 3$). $^{***}p < 0.001$, two-tailed unpaired Student's *t*-test. e) Both of enzyme (green curves) and PTX (blue curves) release profiles of SP-NE at different conditions: i) incubation in PB at pH 7.4 with or without 50 μM H_2O_2 for 24 h, mimicking physiological and tumor extracellular ROS-abundant conditions respectively; ii) incubation in PB at pH 7.4 or 5.0 for another 24 h, mimicking physiological and tumor intracellular acidic conditions respectively ($n = 3$). $^{***}p < 0.001$, one-way ANOVA, Tukey's post-hoc analysis.

adopted and cultured on methacrylated gelatin gels (5.0 kPa) containing 50 μM H_2O_2, which mimics TME with stiff ECM and abundant ROS content. To track the cellular internalization profiles of SP-NG in MCF-7 cells seeded on methacrylated gelatin gels (5.0 kPa), Cy5-labeled polymer Cy5-dPG(N_3)-ace-PTX was synthesized and utilized to construct SP-NG (SP^{Cy5}-NG). The cellular uptake of SP^{Cy5}-NG at the presence of 50 μM H_2O_2 was quantitatively evaluated in MCF-7 cells via flow cytometry. A gradual increase trend of SP^{Cy5}-NG internalization in MCF-7 cells was observed as time prolonged. In detail, Cy5 level in SP^{Cy5}-NG treated cells at 4 h was 1.5-fold, 3.1-fold, and 22.1-fold higher than that at 2 h, 1 h, and 0.5 h respectively (Figure S7, Supporting Information). To distinguish whether collagenase trapped in nanoenzyme was transported to TME before cellular internalization, FITC-collagenase loaded SP^{Cy5}-NG (fluorescently labeled nanoenzyme, SP^{Cy5}-NE^{FITC}) was employed in MCF-7 cells with or without 50 μM H_2O_2 for CLSM observation. As displayed in Figure S8, Supporting Information, only a few FITC signals while strong Cy5 signals of the internalized SP^{Cy5}-NE^{FITC} at the presence of 50 μM H_2O_2 were observed in MCF-7 cells at 2 h, which suggested decrosslinking of SP^{Cy5}-NE^{FITC} and rapid release of FITC-collagenase extracellularly. By contrast, cells treated by SP^{Cy5}-NE^{FITC} without H_2O_2 for 2 h revealed significantly enhanced FITC signals co-located largely with similar Cy5 signals (Figure S8, Supporting Information). At 4 h, stronger Cy5 signals but little FITC signals were detected in SP^{Cy5}-NE^{FITC} plus H_2O_2 group as compared with those at 2 h, while both of stronger Cy5 and FITC signals were observed in SP^{Cy5}-NE^{FITC} without H_2O_2 group as compared with those at 2 h (Figure S8, Supporting Information). Collectively, in the micromilieus containing 50 μM H_2O_2 which mimics ROS-abundant TME, FITC-collagenase could be efficiently released from nanoenzymes before cellular internalization. Next, we assessed the proteolytic activities of nanoenzyme on mechanical performances of methacrylated gelatin matrices. As expected, the elastic modulus of 15% hydrogel decreased to about 1.5 and 0.5 kPa after incubation with S-NE in H_2O_2-containing media for 5, and 10 h, respectively (Figure S9, Supporting Information). To

evaluate if the mechanical change of the matrices triggered by nanoenzyme could affect a series of cell behaviors including cell morphology, spreading, and proliferation, we conducted confocal imaging to visualize the cell morphology and spreading. After incubation with S-NE (collagenase: 0.1 mg mL^{-1}) at the presence of H_2O_2, MCF-7 human breast tumor cells cultured on the stiff gels (5.0 kPa) displayed round morphologies with small and impaired actin bundles, which is similar to the group treated with SP-NE at the same enzyme concentration and the cells cultured on soft gels (0.5 kPa) (**Figure 3**a). By comparison, the untreated cells were well spread with a clear and better-aligned actin meshwork (Figure 3a). In addition, the quantitative results showed drastically decreased cell spreading areas of S-NE-treated MCF-7 cells in a dose-dependent manner, and

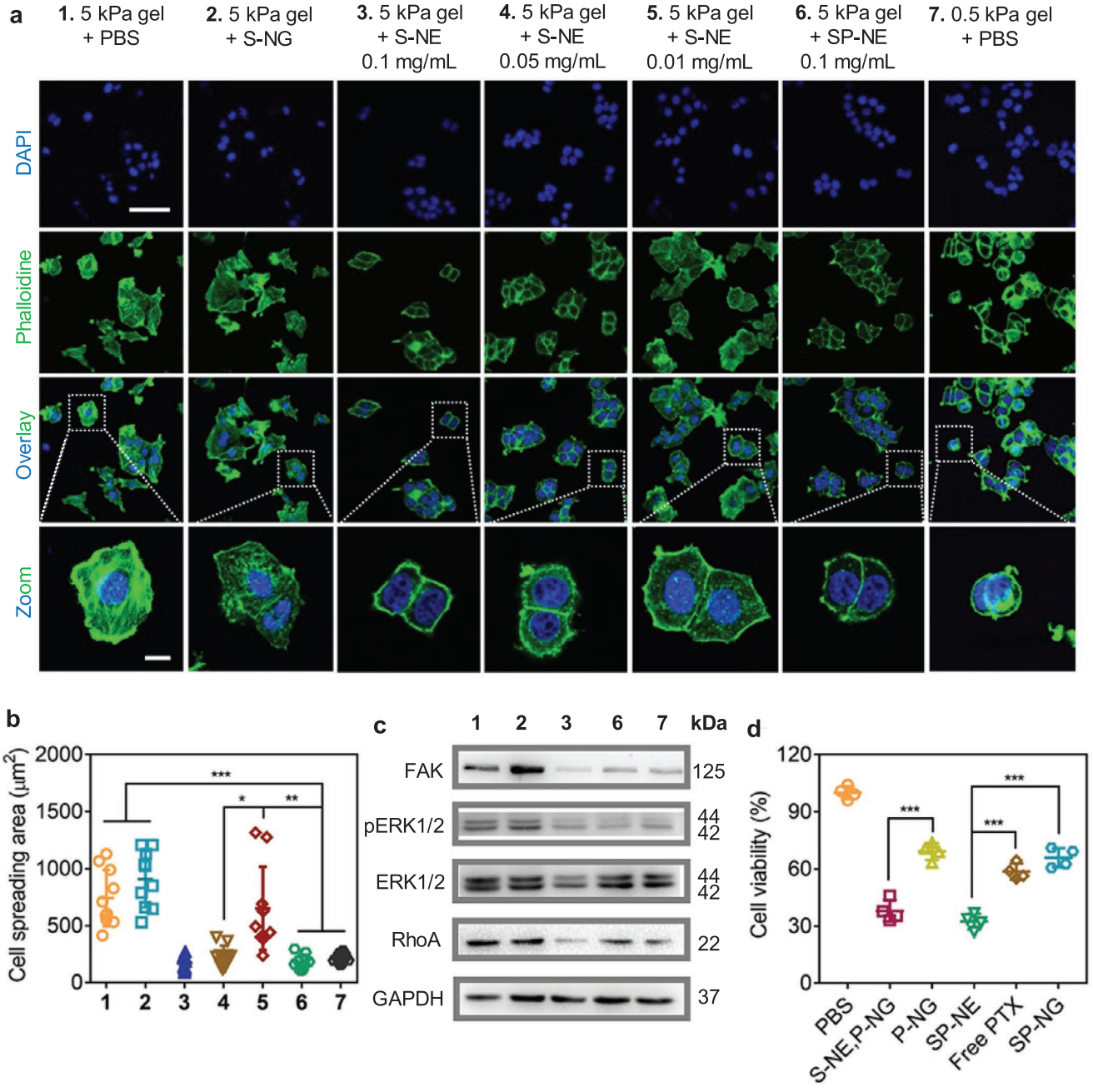

Figure 3. In vitro characterization of SP-NE in MCF-7 cells seeded on methacrylated gelatin gels containing 50 μM H_2O_2, which mimics TME. a) CLSM images depicting actin meshwork change of MCF-7 cells. Cells were treated with different groups for 4 h, and incubated in fresh cell culture media for another 48 h. Blue signals, nucleus; green signals, F-actin. Scale bar: 50 μm; scale bar in inserted images: 10 μm. b) Quantification of cell spreading areas from CLSM images in (a) ($n = 10$). $^{*}p < 0.05$; $^{**}p < 0.01$; $^{***}p < 0.001$, one-way ANOVA, Tukey's post-hoc analysis. c) Western blotting results of expressions of proteins FAK, RhoA mediating actin assembly, as well as pERK 1/2 involved in cell mitosis in MCF-7 cells receiving the above treatments. d) CCK-8 assays of MCF-7 cells treated by different groups (collagenase: 0.05 mg mL^{-1}, PTX: 3 μg mL^{-1}) for 48 h ($n = 4$). For S-NE plus P-NG group, cells were pretreated with S-NE for 4 h and replaced with P-NG for another 48 h incubation. $^{***}p < 0.001$, one-way ANOVA, Tukey's post-hoc analysis.

the cell spreading areas of both S-NE and SP-NE groups were about 200 μm^2 versus 741 μm^2 of untreated cells and 908 μm^2 of empty nanocarrier (S-NG) treated cells (Figure 3b). These data suggested S-NE and SP-NE softened the mechanical strength of the matrix, and subsequently compromised the cell spreading degree and the cytoskeleton network, verifying our hypothesis.

The extrinsic mechanical cues from ECM can be associated with cellular actomyosin cytoskeleton via focal adhesions, which contain vinculin and other mechano-sensing complex. The immunofluorescent images showed a decline of vinculin levels in MCF-7 cells seeded on stiff gels (5.0 kPa) containing 50 μM H_2O_2 treated by SP-NE relative to untreated cells on stiff gels (5.0 kPa), which is in agreement with cytoskeleton imaging results (Figure S10, Supporting Information). The downstream proteins FAK and RhoA also play important roles in sensing mechanical signaling transduction and sustaining cytoskeletal integrity.[38,39] We then assessed whether the integrin-FAK-RhoA signaling axis was affected upon S-NE and SP-NE treatment. Western blot analysis was carried out in MCF-7 cells seeded on methacrylated gelatin gels containing 50 μM H_2O_2 following different treatments. The results revealed that the protein levels of FAK and RhoA, which fundamentally manipulates cellular behaviors,[40,41] were severely diminished in cells treated with S-NE, SP-NE, and collagenase (Figure 3c). Furthermore, another feedback loop of integrin-FAK-pERK 1/2, which is crucial for mitosis and cell proliferation,[42] was also identified to have been weakened (Figure 3c). Altogether, our finding uncovered the molecular mechanism underlying SP-NE (or S-NE)-induced cell shrinkage and cytoskeletal dampening. Hence, TME primed with SP-NE (or S-NE) may provide cancer cells a less favorable environment, eventually improving chemosensitivity within cancer cells.

To verify our hypothesis, S-NE pre-treated MCF-7 cells were further treated with crosslinked dPG(N_3)-ace-PTX nanogels (P-NG) and the cell viabilities were tested by cell counting kit-8 (CCK-8). As shown in Figure 3d, S-NE pre-treated MCF-7 cells were demonstrated to be more sensitive to P-NG treatment with a 30% diminished cell viability as compared to the cells treated by P-NG only. Remarkably, SP-NE composed of 50% S-NE for TME mechanical remodeling and 50% P-NG for cellular chemotherapy was also employed on MCF-7 cells for CCK-8 assays. A significant decline of cell viability was observed for cells treated with SP-NE (32% cell viability), which was much lower than free PTX (59% cell viability) and SP-NG (66% cell viability) groups at a PTX dosage of 3 μg mL^{-1} (Figure 3d), substantiating the sensitization and efficacy of SP-NE in killing cancer cells. The potential toxicities of the nanocarriers without PTX or collagenase (S-NG) and the nanoenzyme without PTX (S-NE) were also tested and demonstrated to show little effect on MCF-7 cell proliferation (Figure S11, Supporting Information). Collectively, SP-NE combining the functions of both ECM mechanical remodeling and the following chemo-sensitization in killing cells, offers a new therapeutic avenue.

2.3. SP-NE for Eliciting In Vivo ECM Mechanical Remodeling

Next, we attempted to utilize the novel SP-NE systems for in vivo antitumor therapy. First of all, we performed a time-lapse monitoring of DIR-loaded SP-NG (SP-NG/DIR) distribution throughout MCF-7 tumor-bearing mice following i.v. injection. The in vivo fluorescence images showed an evident DIR fluorescence in the tumor site at 6 h post injection, the tumor fluorescence level increased as time prolonged, indicating an efficient tumor-homing property of SP-NG (**Figure 4**a). In addition, ex vivo imaging and the corresponding fluorescence quantitative results at 24 h also pointed to a same trend that the tumor accumulation of SP-NG/DIR was significantly higher relative to that in most organs including heart, spleen, lung, and kidney (Figure 4b,c). Quantitation of the PTX distribution profiles indicated the intratumoral PTX level at 24 h post i.v. injection of SP-NG reached 5.6% of injected dose per gram of tissue (%ID g^{-1}) (Figure S12, Supporting Information).

After that, SP-NE system was subjected to MCF-7 tumor-bearing mice for ECM mechanical remodeling. It is well known that collagen is the major ingredient of ECM, and the degradation of collagen in the ECM by the enzymes would lead to remission of the ECM tension. Using rheology, we found that the elastic modulus of MCF-7 tumors after incubation with SP-NE, S-NE, and collagenase decreased to 1181, 884, and 571 Pa versus 4300–6900 Pa in tumors before incubation (Figure 4d). Furthermore, we measured collagen I levels in MCF-7 tumors via immunofluorescence staining after different treatments. Treatments of SP-NE, S-NE, and collagenase resulted in massively declined red fluorescence degrees, which correspond to collagen I levels (Figure 4e). ELISA analysis revealed collagen I levels in MCF-7 tumors were remarkably decreased by 61.1% for SP-NE, 64.0% for S-NE, and 73.6% for collagenase versus the control group (Figure 4f). These results indicated that SP-NE and S-NE could digest the collagen in ECM and relieve the mechanical strength of ECM.

2.4. In Vivo Therapeutic Effects of SP-NE

To validate whether SP-NE elicited ECM softening and the following PTX release can promote antitumor activities in vivo, we adopted subcutaneous MCF-7 human breast tumor xenografted mice models. The tumor-bearing mice were treated with S-NE, free PTX, SP-NG, S-NE plus P-NG (mice were pretreated with S-NE for 12 h, and then treated with P-NG), or SP-NE respectively (collagenase dosage: 10 mg kg^{-1}, PTX dosage: 3 mg kg^{-1}, n = 6) and the injections were administrated every 3 days. From our analysis on day 19 post treatment initiated, mice receiving S-NE showed a slight decline of tumor growth with tumor inhibition of about 15.1% (**Figure 5**a,b). Particularly, both of the S-NE plus P-NG and SP-NE showed similar effects and produced effective inhibition of tumor growth with suppression ratios of 84.9% and 87.1% separately on day 19, which were far more effective than free PTX (41.1% on day 19) and SP-NG (56.7% on day 19) groups (Figure 5a,b). All groups showed little effect on mice body weight change (Figure S13, Supporting Information) and the liver tissues according to histological analysis of the liver on day 19 (Figure S14, Supporting Information), indicating a good safety of SP-NE in mice.

On day 19, the tumors of all groups were harvested and subjected to histological analysis. The results further manifested

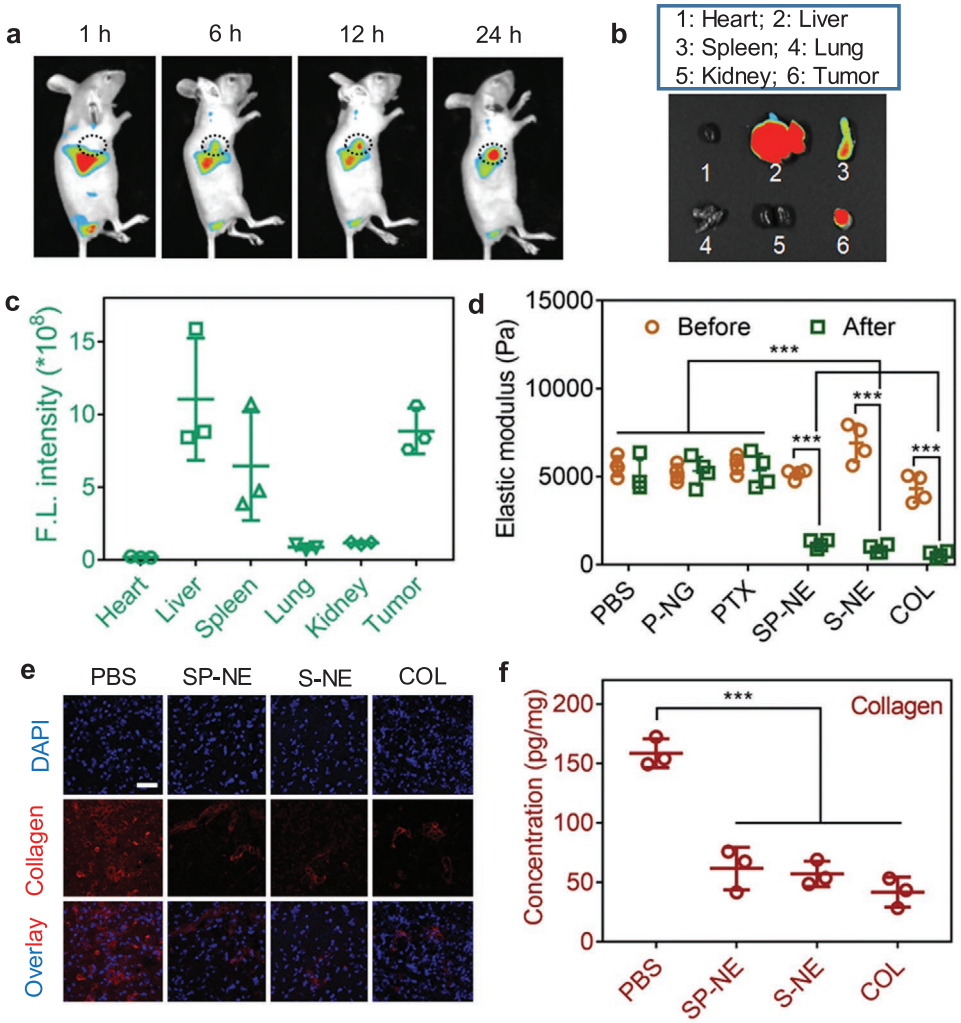

Figure 4. In vivo characterization of SP-NE. a) In vivo fluorescence images of MCF-7 tumor-bearing mice receiving DIR-loaded SP-NG at different time points. b) Ex vivo fluorescence images of the major organs or tissues treated with DIR-loaded SP-NG at 24 h. c) Quantification of fluorescence intensity of the organs or tissues according to ex vivo fluorescence images ($n = 3$). d) Elastic modulus (G') of MCF-7 tumors before and after different treatments at a collagenase concentration of 0.05 mg mL^{-1} at 37 °C for 10 h measured by rheology at a strain of 0.1% and a frequency of 1 Hz ($n = 4$). $^{***}p < 0.001$, two-way ANOVA, Bonferroni's post-hoc analysis. e) CLSM immunofluorescence images of collagen expression in MCF-7 tumors treated by different groups. Blue signals, nucleus; red signals, collagen ($n = 6$). Scale bar: 100 µm. f) ELISA analysis of collagen levels in MCF-7 tumors treated by different groups ($n = 3$). $^{***}p < 0.001$, one-way ANOVA, Tukey's post-hoc analysis.

that both S-NE plus P-NG and SP-NE treatments caused severe damage to tumor tissues with the highest levels of green fluorescence and the extensive necrotic cells as revealed by TUNEL and H&E staining, respectively (Figure 5c and Figure S14, Supporting Information).

2.5. In Vivo Validation of SP-NE for Sensitizing in Combating Tumors

Finally, we tried to validate our assumption that the enhanced chemotherapeutic efficacy of SP-NE was attributed to the interference of integrin-FAK-RhoA and integrin-FAK-pERK 1/2 signaling in vivo. To this end, the tumor blocks of each group were collected for immunofluorescence staining. Three key players (vinculin, RhoA and pERK 1/2) that mediated cellular mechanical signaling and the structure of cytoskeletons were specifically labeled for CLSM observation. The signals of vinculin, RhoA, and pERK 1/2 were widely distributed in the whole tumor with a relatively high intensity in PB saline (PBS) group but were barely distributed in the tumors with lower intensities in the SP-NE-, S-NE-, and collagenase-treated groups (Figure 5d and Figure S15, Supporting Information). Consistently, ELISA analysis revealed shrinkages of about 55.4% for vinculin expression, 55.8% for RhoA expression, and 63.5% for pERK 1/2 expression in SP-NE-treated group relative to the PBS group (Figure 5e,f and Figure S15, Supporting Information). The significant regression of vinculin, RhoA and pERK 1/2 expression by SP-NE treatment thereby provided a molecular mechanism of enhanced in vivo anti-tumor outcome treated by SP-NE.

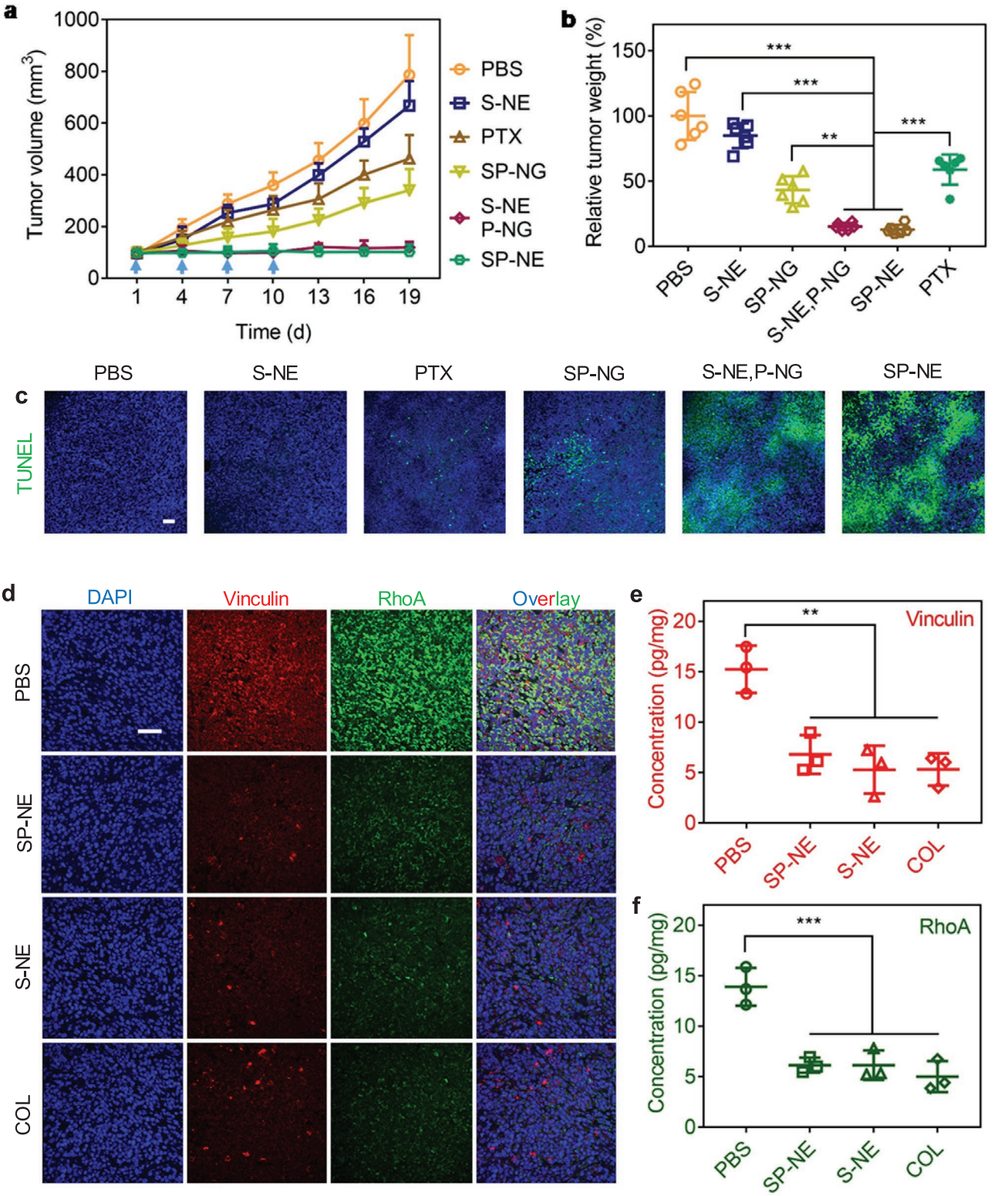

Figure 5. In vivo therapeutic efficacy of SP-NE in MCF-7 tumor-bearing mice models. a) Tumor volume change of different groups ($n = 6$). Mice were intravenously administrated equivalent collagenase dosage of 10 mg kg^{-1} and PTX dosage of 3 mg kg^{-1} on days 1, 4, 7, and 10. b) Relative tumor weight of different groups at the end of the experiment ($n = 6$). $^{**}p < 0.01$; $^{***}p < 0.001$, one-way ANOVA, Tukey's post-hoc analysis. c) TUNEL staining of MCF-7 tumors from different groups at the end of the experiment. Scale bar: 50 µm. d) CLSM immunofluorescence images of MCF-7 tumors from different groups at the end of the experiments. Blue signals, nucleus; red signals, vinculin; green signals, RhoA. Scale bar: 100 µm. e,f) ELISA analysis of vinculin (e) and RhoA (f) levels in MCF-7 tumors treated by different groups at the end of the experiments ($n = 3$). $^{**}p < 0.01$; $^{***}p < 0.001$, one-way ANOVA, Tukey's post-hoc analysis.

3. Conclusion

In this work, a ROS-responsive nanogel architecture combining collagenase and a PTX prodrug (SP-NE) was successfully developed for ECM mechanical remodeling and enhanced chemotherapy sensitized by relieved tumor stress. Collagenase was efficiently released from SP-NE due to abundant ROS in TME for ECM digestion, resulting in about 10-fold reduction in tumor stiffness as well as 4-fold shrinkage in cell spreading areas, which in turn greatly aided chemotherapeutics of PTX in cancer cells with 30% diminishment of cell viability relative to free PTX. A significant tumor inhibition of 87.1% was achieved in MCF-7 tumor-bearing mice receiving SP-NE at a low dosage of 3 mg equiv. PTX kg^{-1}. Furthermore, the underlying mechanism was proposed and verified that the SP-NE treatment downregulated cellular mechanical signaling pathways of integrin-FAK-RhoA in increasing F-actin assembly dynamics and integrin-FAK-pERK 1/2 in promoting mitosis via softening ECM both in vitro and in vivo. Therefore, our approach enriches arsenal of TME modifying strategies for better cancer treatment outcomes. Our research extends the understanding on mechano-biology of TME and can guide the design of nanomedicines for cancer therapy.

4. Experimental Section

Materials: 2-Iminothiolane hydrochloride (Traut's reagent, 98%), paclitaxel (PTX, 95%), *p*-toluenesulfonic acid monohydrate (*p*-TSA, 99%), oxalyl chloride (99%), propargyl alcohol (99%), collagenase (95%), gelatin, methacrylic anhydride (94%) were bought from Sigma-Aldrich and used as received. Polymers dendritic azido polyglycerol sulfate (dPGS-N_3, 10 kDa, 10% azidation, 82% sulfation), dendritic azido polyglycerol (dPG-N_3, 10 kDa, 10% azidation), gelatin methacrylate (degree of substitution: 70%), and VEA, were synthesized according to previous reports.[35,43]

Preparation and Characterization of SP-NE: For preparation of SP-NE, polymers dPGS-N_3 (50 µL, 10 mg mL^{-1}), dPG(N_3)-ace-PTX (50 µL, 10 mg mL^{-1}), and the crosslinker oxalyl dialkynyl (4 µL, 10 mg mL^{-1}) were first dissolved in DMSO, and then the mixture was added into 2.5 mL PB (pH 7.4, 5 mM) containing collagenase (0.12 mg mL^{-1}) dropwise and the whole solution was stirred overnight for a complete crosslinking followed by dialysis against PB (pH 7.4, 5 mM) for 8 h to remove unentrapped collagenase and DMSO. The size and morphology were characterized via DLS and TEM.

Enzyme loading capacity was determined to be 16.8 wt% via BCA assays, and fluorescein isothiocyanate-labeled collagenase (FITC-COL) was used for in vitro enzyme release studies. Typically, 0.5 mL SP-NE solution entrapped with FITC-COL was added in a dialysis tube (Spectra/Pore, MWCO 1 000 000) followed by immersion in 20 mL PB (pH 7.4) at 37 °C either with or without H_2O_2 (50 µM) for 24 h. Afterward, the dialysis media was replaced with PB at pH 7.4 or acetate buffer at pH 5.0 for another 24 h. At certain time intervals, 6 mL of release media was collected and detected via HPLC (Shimadzu LC20AD, Japan) and fluorometry (Agilent Technologies, USA). The experiments were performed in triplicate.

In Vitro Characterization of SP-NE: To mimic tumor extracellular matrix, gelatin methacrylate hydrogel with mechanical strength of 5 kPa was fabricated as cell culture matrix. Briefly, 100 µL gelatin methacrylate solution (150 mg mL^{-1}) blended with 0.5% (w/v) lithium phenyl-2,4,6-trimethyl-benzoyl-phosphinate was irradiated under 365 nm for 10 min using a UV box. The mechanical features of methacrylated gelatin gels were measured via Malvern rheometer kinexus equipped with 8 mm parallel-plate geometry. Matrix stiffness data was recorded from frequency sweeps performed at a strain of 0.1% and a frequency of 1 Hz. The enzymatic effects on the stiffness of methacrylated gelatin gels were conducted by incubating gels with S-NE in medium containing 50 µM H_2O_2 at a collagenase concentration of 0.05 mg mL^{-1} at 37 °C for 5 h and 10 h respectively. The formed gels were then washed with PB for three times, and replaced with cell culture media containing 50 µM H_2O_2 for the following in vitro experiments. Herein, human breast tumor MCF-7 cells were adopted and cultured in DMEM (high glucose, Gibco) supplemented with 10% 10% FBS (Gibco), 100 µg mL^{-1} penicillin, and 100 U mL^{-1} streptomycin (Gibco).

MCF-7 cells were seeded on methacrylated gelatin gels containing 50 µM H_2O_2 coating on a coverslip with a diameter of 12 mm at a density of 5000 cells cm^{-2}. 12 h later, cells were treated with PBS, S-NG, S-NE, and SP-NE for 4 h respectively, followed by replacement of fresh cell culture media for another 48 h incubation. To visualize cell morphologies, cells from different groups were fixed with 1% paraformaldehyde for 30 min and then permeabilized with 0.1% Triton-100 in PBS for 1 h. Afterwards the cells were stained with 4′-6-diamidino-2-phenylindole (DAPI, 1:1000, Thermo Fischer Scientific, USA) and Alexa Fluor 488 phalloidin (fluorescent phalloidin was used for visualizing F-actin, 1:500, Thermo Fischer Scientific, USA) in PBS for 10 min. Finally, the cells were imaged by a confocal microscope (SP8, Leica, Germany). Cell spreading area was quantified according to F-actin signals and analyzed via Image J ($n = 10$).

In Vivo Antitumor Activity: The therapeutic effects of SP-NE mediated ECM degradation in TME and chemotherapy in tumor cells were performed in a MCF-7 human breast tumor-bearing mice model by injecting MCF-7 cells (5×10^6 cells per mouse) into the right hind flank of the female nude mice. The animal experiments were performed in accordance with the protocols approved by China Pharmaceutical University. When the tumor volume reached 100 mm^3, mice were randomly divided into 6 groups ($n = 6$) and individually administrated with PBS, S-NE, PTX, SP-NG, S-NE plus P-NG, and SP-NE intravenously (collagenase dosage: 10 mg kg^{-1}, PTX dosage: 3 mg kg^{-1}). For S-NE plus P-NG group, mice were treated with S-NE and subsequent P-NG at 12 h later. The treatments repeated every 3 days and ended at day 10. Tumor volume and body weight of mice in each group were observed and recorded. At day 19 post treatment initiated, tumor blocks of mice were collected and weighed for tumor inhibition analysis.

In Vivo Mechanical Remodeling of ECM: The mechanical properties of the tumor tissues with different treatment were also measured via shear rheology. Briefly, the tumor samples were freshly resected from subcutaneous human breast MCF-7 tumor-bearing mice, and obtained as a cylindrical shape with a size of 8 mm in diameter and 2 mm in thickness for rheological measurement. The excised tumor samples were then incubated with PBS, P-NG, free PTX, SP-NE, S-NE, and free collagenase in medium containing 50 µM H_2O_2 at a collagenase concentration of 0.05 mg mL^{-1} at 37 °C for 10 h respectively. Afterward all the tumor samples were processed for measurement again. Elastic modulus (G') of tumor tissues was determined by the frequency sweeps performed at a strain of 0.1% and a frequency of 1 Hz. To further elucidate the effect of nanoenzymes on tumor mechanical stiffness in vivo, MCF-7 tumor-bearing mice with tumor volume of about 200 mm^3 were injected with PBS, SP-NE, S-NE, and collagenase individually. 2 days later, all the tumor tissues were collected, embedded in the paraffin, and sliced. After incubation in 5% BSA solution to block nonspecific binding, tumor sections were stained with specific antibody of collagen I (1:500, Abcam, ab34710, UK), and then incubated with Alexa Fluor 488-labeled secondary antibody (1: 1000, Thermo Fischer Scientific, USA). The cell nuclei were stained with DAPI, and the tumor samples were visualized under CLSM. For the quantitative determination of collagen I level in tumors treated by different groups, a commercially available ELISA kit for collagen type I (Col I, CUSABIO, P. R. China) was used, the tumor tissue homogenates collection and the assay procedure were conducted according to the manufacturer's instructions.

To verify the underlying mechanism of SP-NE modulated mechanical signaling pathways of integrin-FAK-RhoA and integrin-FAK-pERK 1/2 in vivo, the sectioned slices were also subjected to anti-vinculin (1: 100,

Abcam, ab129002, UK), anti-RhoA (1:150, Abcam, ab187027, UK) or anti-pERK 1/2 (1:100, Sigma, USA) antibodies, and following Alexa Fluor 488 and 647-labeled secondary antibodies (1:400, Invitrogen) solution containing DAPI after incubation in 5% BSA solution. Relative expressions of vinculin, RhoA and pERK 1/2 were observed under CLSM. For the quantitative determination of vinculin, RhoA, and pERK 1/2 expressions in tumors treated by different groups, commercially available ELISA kits for vinculin (VCL, CUSABIO, P. R. China), RhoA (FineTest, P. R. China), and pERK1/2 (Abcam, ab176640, UK) were used, the tumor tissue homogenates collection and the assay procedure were conducted according to the manufacturer's instructions.

Statistical Analysis: Data were presented as mean ± standard deviation. For comparisons, the experimental data was analyzed using a two-tailed unpaired Student's *t*-test, one-way ANOVA with Tukey's post-hoc test or two-way ANOVA with Bonferroni's post-hoc test. $p < 0.05$ was considered as statistically significant ($*p < 0.05$, $**p < 0.01$, $***p < 0.001$).

Supporting Information

Supporting Information is available from the Wiley Online Library or from the author.

Acknowledgements

This work was funded by the German Science Foundation (DFG) within the SFB 765, the National Natural Science Foundation of China (NSFC 51803238, 51973233, 51703244, and 21878337), the Natural Science Foundation of Jiangsu Province (BK20170730), Jiangsu Specially-Appointed Professor Program to W.C. The authors would like to acknowledge the assistance of the Core Facility BioSupraMol (Freie Universität Berlin, Germany). The authors would like to thank Dr. Pamela Winchester for language polishing this manuscript.

Open access funding enabled and organized by Projekt DEAL.

Conflict of Interest

The authors declare no conflict of interest.

Keywords

mechanical remodeling, nanomedicine, sensitized chemotherapy, tumor microenvironment, tumor stiffness

Received: September 3, 2020
Published online: October 2, 2020

[1] Y. S. Youn, Y. H. Bae, *Adv. Drug Delivery Rev.* **2018**, *130*, 3.
[2] J. Shi, P. W. Kantoff, R. Wooster, O. C. Farokhzad, *Nat. Rev. Cancer* **2017**, *17*, 20.
[3] S. Mitragotri, D. G. Anderson, X. Chen, E. K. Chow, D. Ho, A. V. Kabanov, J. M. Karp, K. Kataoka, C. A. Mirkin, S. H. Petrosko, J. Shi, M. M. Stevens, S. Sun, S. Teoh, S. S. Venkatraman, Y. Xia, S. Wang, Z. Gu, C. Xu, *ACS Nano* **2015**, *9*, 6644.
[4] C. Deng, Y. Jiang, R. Cheng, F. Meng, Z. Zhong, *Nano Today* **2012**, *7*, 467.
[5] Y. Dai, C. Xu, X. Sun, X. Chen, *Chem. Soc. Rev.* **2017**, *46*, 3830.
[6] J. Liu, Q. Chen, L. Feng, Z. Liu, *Nano Today* **2018**, *21*, 55.
[7] H. S. El-Sawy, A. M. Al-Abd, T. A. Ahmed, K. M. El-Say, V. P. Torchilin, *ACS Nano* **2018**, *12*, 10636.
[8] B. Chen, W. Dai, B. He, H. Zhang, X. Wang, Y. Wang, Q. Zhang, *Theranostics* **2017**, *7*, 538.
[9] M. Overchuk, G. Zheng, *Biomaterials* **2018**, *156*, 217.
[10] J. Schrader, T. T. Gordon-Walker, R. L. Aucott, M. van Deemter, A. Quaas, S. Walsh, D. Benten, S. J. Forbes, R. G. Wells, J. P. Iredale, *Hepatology* **2011**, *53*, 1192.
[11] P. Lu, V. M. Weaver, Z. Werb, *J. Cell Biol.* **2012**, *196*, 395.
[12] H. Mohammadi, E. Sahai, *Nat. Cell Biol.* **2018**, *20*, 766.
[13] V. Seewaldt, *Nat. Med.* **2014**, *20*, 332.
[14] O. Chaudhuri, S. T. Koshy, C. B. da Cunha, J.-W. Shin, C. S. Verbeke, K. H. Allison, D. J. Mooney, *Nat. Mater.* **2014**, *13*, 970.
[15] M. C. Lampi, C. A. Reinhart-King, *Sci. Transl. Med.* **2018**, *10*, eaao0475.
[16] S. Ishihara, D. R. Inman, W.-J. Li, S. M. Ponik, P. J. Keely, *Cancer Res.* **2017**, *77*, 6179.
[17] C. C. DuFort, M. J. Paszek, V. M. Weaver, *Nat. Rev. Mol. Cell Biol.* **2011**, *12*, 308.
[18] J. Zhu, M. Xu, M. Gao, Z. Zhang, Y. Xu, T. Xia, S. Liu, *ACS Nano* **2017**, *11*, 2637.
[19] A. Marturano-Kruik, A. Villasante, K. Yaeger, S. Ambati, A. Chramiec, M. Raimondi, G. Vunjak-Novakovic, *Biomaterials* **2018**, *150*, 150.
[20] J. Li, C. Xie, J. Huang, Y. Jiang, Q. Miao, K. Pu, *Angew. Chem., Int.. Ed.* **2018**, *57*, 3995.
[21] A. Parodi, S. G. Haddix, N. Taghipour, S. Scaria, F. Taraballi, A. Cevenini, I. K. Yazdi, C. Corbo, R. Palomba, S. Z. Khaled, J. O. Martinez, B. S. Brown, L. Isenhart, E. Tasciotti, *ACS Nano* **2014**, *8*, 9874.
[22] H. Zhou, Z. Fan, J. Deng, P. K. Lemons, D. C. Arhontoulis, W. B. Bowne, H. Cheng, *Nano Lett.* **2016**, *16*, 3268.
[23] T. Tan, H. Hu, H. Wang, J. Li, Z. Wang, J. Wang, S. Wang, Z. Zhang, Y. Li, *Nat. Commun.* **2019**, *10*, 3322.
[24] J. D. Martin, M. Panagi, C. Wang, T. T. Khan, M. R. Martin, C. Voutouri, K. Toh, P. Papageorgis, F. Mpekris, C. Polydorou, G. Ishii, S. Takahashi, N. Gotohda, T. Suzuki, M. E. Wilhelm, V. A. Melo, S. Quader, J. Norimatsu, R. M. Lanning, M. Kojima, M. D. Stuber, T. Stylianopoulos, K. Kataoka, H. Cabral, *ACS Nano* **2019**, *13*, 6396.
[25] H. Wang, X. Han, Z. Dong, J. Xu, J. Wang, Z. Liu, *Adv. Funct. Mater.* **2019**, *29*, 1902440.
[26] Y. Liu, Y. Jiang, M. Zhang, Z. Tang, M. He, W. Bu, *Acc. Chem. Res.* **2018**, *51*, 2502.
[27] J. Conniot, A. Scomparin, C. Peres, E. Yeini, S. Pozzi, A. I. Matos, R. Kleiner, L. I. Moura, E. Zupančič, A. S. Viana, H. Doron, P. M. P. Gois, N. Erez, S. Jung, R. Satchi-Fainaro, H. F. Florindo, *Nat. Nanotechnol.* **2019**, *14*, 891.
[28] J. Insua-Rodriguez, T. Oskarsson, *Adv. Drug Delivery Rev.* **2016**, *97*, 41.
[29] K. R. Levental, H. Yu, L. Kass, J. N. Lakins, M. Egeblad, J. T. Erler, S. F. T. Fong, K. Csiszar, A. Giaccia, W. Weninger, M. Yamauchi, D. L. Gasser, V. M. Weaver, *Cell* **2009**, *139*, 891.
[30] A. Zinger, L. Koren, O. Adir, M. Poley, M. Alyan, Z. Yaari, N. Noor, N. Krinsky, A. Simon, H. Gibori, M. Krayem, Y. Mumblat, S. Kasten, S. Ofir, E. Fridman, N. Milman, M. M. Lübtow, L. Liba, J. Shklover, J. Shainsky-Roitman, Y. Binenbaum, D. Hershkovitz, Z. Gil, T. Dvir, R. Luxenhofer, R. Satchi-Fainaro, A. Schroeder, *ACS Nano* **2019**, *13*, 11008.
[31] J. Liu, L. Tian, R. Zhang, Z. Dong, H. Wang, Z. Liu, *ACS Appl. Mater. Int.* **2018**, *10*, 43493.
[32] A. Pan, Z. Wang, B. Chen, W. Dai, H. Zhang, B. He, X. Wang, Y. Wang, Q. Zhang, *Drug Delivery* **2018**, *25*, 1495.
[33] Y. Zhong, K. Goltsche, L. Cheng, F. Xie, F. Meng, C. Deng, Z. Zhong, R. Haag, *Biomaterials* **2016**, *84*, 250.

[34] A. Costa, A. Scholer-Dahirel, F. Mechta-Grigoriou, *Semin. Cancer Biol.* **2014**, *25*, 23.
[35] D. Groeger, M. Kerschnitzki, M. Weinhart, S. Reimann, T. Schneider, B. Kohl, W. Wagermaier, G. Schulze-Tanzil, P. Fratzl, R. Haag, *Adv. Healthcare Mater.* **2014**, *3*, 375.
[36] D. Lee, S. Bae, Q. Ke, J. Lee, B. Song, S. A. Karumanchi, G. Khang, H. S. Choi, P. M. Kang, *J. Controlled Release* **2013**, *172*, 1102.
[37] C.-C. Song, F.-S. Du, Z.-C. Li, *J. Mater. Chem. B* **2014**, *2*, 3413.
[38] S. H. Lee, R. Dominguez, *Mol. Cells* **2010**, *29*, 311.
[39] D. Spiering, L. Hodgson, *Cell Adhes. Migr.* **2011**, *5*, 170.
[40] F. J. Sulzmaier, C. Jean, D. D. Schlaepfer, *Nat. Rev. Cancer* **2014**, *14*, 598.
[41] V. T. Chin, C. Vennin, S. C. Warren, M. C. Lucas, D. Herrmann, A. Magenau, P. Melenec, S. N. Walters, G. d. Monte-Nieto, J. R. W. Conway, M. Nobis, A. H. Allam, R. A. McCloy, N. Currey, M. Pinese, A. Boulghourjian, A. Zaratzian, A. A. S. Adam, C. Heu, A. M. Nagrial, A. Chou, A. Steinmann, A. Drury, D. Froio, M. Giry-Laterriere, N. L. E. Harris, T. Phan, R. Jain, W. Weninger, E. J. McGhee, et al., *Sci. Transl. Med.* **2017**, *9*, eaai8504.
[42] W. Zhang, H. T. Liu, *Cell Res.* **2002**, *12*, 9.
[43] J. Zhang, H. Yang, B. E. Abali, M. Li, Y. Xia, R. Haag, *Small* **2019**, *15*, 1901920.